Using Phase Doppler Anemometry and High Speed Imaging to Analyze MDI Spray Plume Dynamics

H.K. Versteeg,[1] G.K. Hargrave,[1] B.J. Myatt,[1] D. Lewis,[2] T. Church,[2] and G. Brambilla[3]

[1] Wolfson School of Mechanical, Electrical and Manufacturing Engineering, Loughborough University, Loughborough, United Kingdom

[2] Chiesi Limited, Chippenham, United Kingdom

[3] Chiesi Farmaceutici SpA, Parma, Italy

KEYWORDS: metered dose inhalers (MDIs), aerosol plume dynamics, phase-Doppler anemometry (PDA), high-speed imaging, particle image velocimetry (PIV)

SUMMARY

Characterization of inhalation aerosols focuses in the first instance on aerodynamic particle size, which is measured using cascade impactors. The aerosol must contain large quantities of particles in the respirable size range 1-5 μm. Deposition on impactor stages depends on the velocity of the particles as well as their size. Pressurized metered dose inhalers (pMDIs) produce very fast-moving spray plumes, so it is important to understand the dynamic nature of droplet formation processes and spray plumes. This paper presents a selection of findings from an optical diagnostics study of aerosol plumes generated by a Bespak 630 series actuator in conjunction with a series of HFA134a placebo formulations containing ethanol up to 20% w/w. Spray plume dynamics in the vicinity of the spray orifice and further downstream were characterized using phase-Doppler anemometry (PDA), high-speed imaging and particle image velocimetry (PIV). The findings demonstrate the complementary capabilities of these instruments. PDA provides simultaneous values of mean droplet size and velocity (and their associated statistics), but it is time-consuming to sample a sufficient number of locations to characterize the rapidly changing spray plume. PIV, on the other hand, provides information on entire flow fields albeit at lower spatial and temporal resolution. PIV and PDA data for the velocity of various spray plumes were found to be in good

agreement, which validates both techniques. High-speed imaging also captures the overall characteristics of the plume. The diffraction limit of the optical configuration used for imaging is around 10 μm, so it is not possible to observe respirable droplets individually. However, the dynamics and trajectories of larger droplets can be studied. Larger droplets were found to be produced by highly localized atomization processes, so the resulting droplets can be easily missed or undersampled in PDA surveys.

These results suggest that further research on pMDI sprays with these combined tools will provide useful insights into the processes responsible for changes in droplet size *and* velocity, and can be expected to make a major contribution to improving the development of the next generation of pMDI inhalers.

INTRODUCTION

The active pharmaceutical ingredient (API) of respirable aerosols produced by pMDIs is dissolved or suspended in hydrofluoroalkane (HFA) propellant prior to release from the valve. Partial evaporation of the volatile propellant provides the driving energy for the emission of the drug dose and fragmentation of liquid bulk. pMDI aerosols predominantly consist of droplets with sizes between 1 and 5 μm. Larger droplets are likely to deposit on the device or in the patient's mouth and throat.

The short duration of individual spray emission events and the low thermal conductivity of pMDI actuator materials cause the HFA propellant evaporation to be (almost) unaffected by heat transfer with the actuator [1]. Under these (almost) adiabatic conditions, the aerosol droplets at the exit of the spray orifice will be cooled and contain a substantial fraction of unevaporated propellant [2]. As the aerosol plume mixes with air in the device mouthpiece, the remaining liquid propellant will evaporate. This process was studied in detail by Stein and Myrdal [2, 3], who measured the residual size of aerosol droplets using an aerodynamic particle sizer (APS) and computed the initial droplet size from the residual size measured by the APS by assuming that no evaporation of propellant or co-solvent takes place inside the actuator.

The mixing between spray plume and the surrounding air also causes a rapid reduction of the aerosol velocity that is inversely proportional to the distance from the spray orifice, as was first documented in [4] for steady chlorofluorocarbon (CFC) aerosol plumes. High-speed imaging was recently used [5] to study these rapid changes in metered HFA sprays without and with glycerol as a non-volatile excipient. A self-similarity model was proposed to predict spray penetration and aerosol plume spreading.

Sprays produced by pMDIs are highly dynamic with large changes of droplet size and spray velocity occurring close to the actuator block and in the mouthpiece region. It is crucial to understand the spray dynamics in sufficient detail to be able to predict changes of particle size and velocity, which influence regional deposition in the lungs and unwanted deposition in the device and oropharynx [1].

MATERIALS AND METHODS

Sprays emitted by a Bespak 630 series pMDI actuator (Bespak, Kings Lynn, UK) were studied. Presspart 19 mL canisters (Presspart, Blackburn, UK), designed to deliver 200 nominal actuations, fitted with a Bespak BK357 metering valve (with polyester stem, metering chamber, and body), were filled with HFA134a/ethanol mixtures (0 to 20% w/w) or pure HFA227ea. A custom-built rig was constructed around a Nanotec L4118S1404-T5X5-A25 linear actuator with SMCI12 stepper motor controller (Nanotec Electronic, Munich, Germany) to actuate the canisters with good repeatability and programmable acceleration, speed, and distance. Earlier studies showed that data from 30 actuation events with 1 minute delay between successive actions was required in order to obtain spray metrics within 1% variance, spray to spray [6]. Measurements of sprays actuated into atmospheric air (temperature 20.5 ± 2˚C) were made by means of PDA, high-speed imaging and PIV.

Phase-Doppler Anemometry (PDA)

A two-component PDA system with an argon-ion laser (emitting at 514.8 nm and 488 nm), described in [7], was used to make surveys of the pMDI aerosol. The droplet velocity and size were measured at a series of locations along the spray orifice axis. Radial surveys were carried out at distances from the nominal spray axis that varied as a function of axial distance from the spray orifice to take into account the widening of the spray. To allow detailed analysis, axial and radial velocity components as well as the number mean droplet size D_{10} and the Sauter mean diameter D_{32} were generated in time bins with a width of 10 ms.

Imaging

High speed images of the spray plumes were recorded at image acquisition rates up to 12 kHz. For far-field laser sheet imaging, the illumination source was a Litron LDY304 Nd:YLF double-pulsed laser (Litron, Rugby, UK) emitting at 527 nm. A planar sheet of laser light was produced using a series of cylindrical and spherical lenses and a slit aperture. LaVision's Imager *Pro* HS-4M (4 Mpixel) camera (LaVision, Göttingen, Germany) equipped with a FX AF-Micro Nikkor 105 mm macrolens (Nikon, Tokyo, Japan) was used to record spray plume images. Cropped image fields of 2016 x 792 pixels were captured by the camera to maximize the image acquisition rate, resulting in an 80 x 30 mm image field.

For near-orifice laser sheet imaging and PIV, the light source was a Litron Nano L 200-15 Nd:YAG PIV laser (Litron, Rugby, UK) emitting at 532 nm. In this set-up, spray plume images were recorded in an image field of 15 x 12 mm with the LaVision's Imager sCMOS (5 Mpixel) camera (LaVision, Göttingen, Germany) equipped with a AF-Micro Nikkor 200 mm macrolens (Nikon, Tokyo, Japan).

To complement the high-speed images and study the aerosols in detail, 50 Mpixel still images were produced with a Canon EOS 5DS R (Canon, Tokyo, Japan) DSLR camera in conjunction with the AF-Micro Nikkor 200 mm macrolens (Nikon, Tokyo, Japan) and extension rings to achieve an image region of 4.0 x 2.7 mm. Images with backlighting used a fluorescein dye cell pumped by a Surelite SSP Nd:YAG Laser (Continuum Lasers, San Jose, CA, USA).

Particle Image Velocimetry (PIV)

For PIV studies, the Litron LDY304 laser was double pulsed with a pulse spacing of 10 μs and the LaVision's Imager *Pro* HS-4M camera with macrolens was operated at a frame rate of 1.608 kHz. Image pairs were analyzed using LaVision's DaVis 8 Flowmaster PIV processing software. The analysis protocol involved one pass with analysis regions of 64 x 64 pixels with 50% overlap followed by a second pass with regions of 32 x 32 pixel region with 50% overlap. A median filter [8] was applied with secondary (or tertiary) vector replacement to eliminate spurious primary velocity vectors.

Finally, to facilitate broader comparisons of the characteristics of sprays with different compositions, averages of spray metrics were computed over the entire spray event (event-average) as well as averages over cross-sectional planes perpendicular to the nominal spray axis (area-average).

RESULTS AND DISCUSSION

Near-orifice Spray Images and Characterization

Figures 1A-1D show high-resolution images of a 4 x 4 mm region immediately adjacent to the spray orifice exit of a HFA134a spray produced by the Bespak 630 actuator at t = 50, 100, 150, and 200 ms after spray was first detected exiting from the spray orifice.

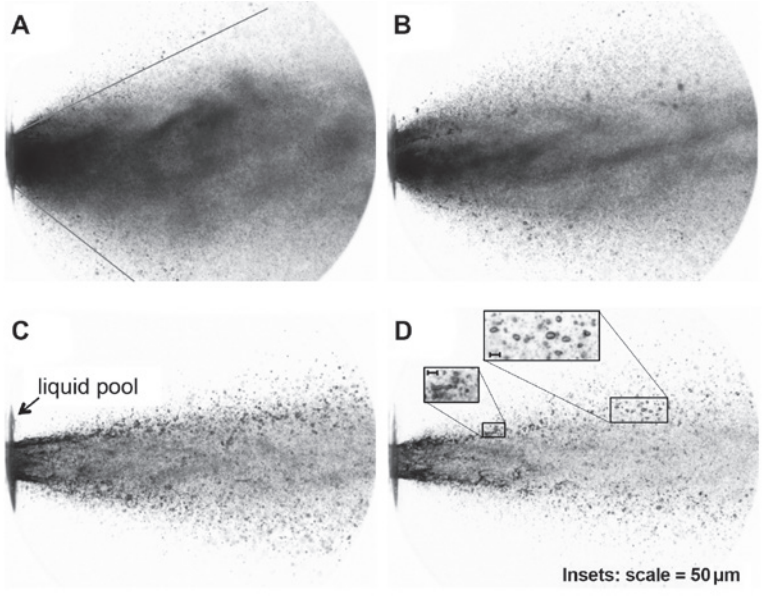

Figure 1. **High-resolution images of HFA134a spray in the near-orifice region. A) 50 ms (spray edge: 98% of pixel intensity counts contained inside indicated boundaries), B) 100 ms, C) 150 ms, D) 200 ms.**

The following spray characteristics were observed in the near-orifice region:

- t = 50 ms: extremely dense spray as it emerges from the spray orifice with cone angle around 60°. The striated appearance indicates emission of small droplets in waves. A small number of larger droplets is formed at the bottom of the spray.
- t = 100 ms: spray density has reduced and the cone angle is 40°. Larger droplets are formed at the spray edge; the spray core mostly contains smaller droplets.
- t = 150-200 ms: annular spray is formed with a cone angle around 20°. Spray density in the core reduces with time. Interaction between a liquid pool on the nozzle exit face and the main jet flow contributes to the formation of irregularly shaped ligaments. Large droplets (size ~20-40 μm) are generated at the edge of the spray; many of these droplets are initially non-spherical.

Figures 2A-2D show laser sheet images of the HFA134a spray for an 80 x 20 mm region at the times t = 50, 100, 150, and 200 ms after the start of flow from the spray orifice. The images show the intensity field of light scattered by spray droplets. The intensity fields were inverted to improve visibility, so dark regions in Figure 2 correspond to high scattered light, i.e., dense sprays and vice-versa.

The characteristics of far-field sprays observed in Figure 2 were as follows:

- Spray density – temporal behavior: scattered light intensity is highest at the start of the spray event and decreases as the spray event progresses, so spray density decreases with time as propellant runs out.
- Spray density – spatial behavior: spray density is always highest near the spray orifice, because spray is diluted by mixing with surrounding air as it progresses downstream.
- Spray cone angle: far-field cone angle is initially around 20° and decreases to 10° during the final stages of the spray event; note that these cone angle values differ from those observed in the high-resolution images, suggesting that different physical processes control the spreading of pMDI sprays in the near-orifice region and the far-field region.
- Droplet motions: more detailed analysis of the images showed that the large droplets, initially detected at the spray edge in high-resolution images (Figure 1), tended to continue along the outer edges of the spray following straight, ballistic trajectories. Smaller droplets follow chaotic trajectories that are caused by the turbulence generated by the interaction between the spray and the surrounding air. The smallest droplets will more or less follow the vertical turbulent motions and will be mixed thoroughly throughout the spray.

PIV – Spray Dynamics: Velocity Field

Each of the far-field images presented above were one of a pair produced with the double-pulsed laser system. Image pairs were analysed using the PIV analyser. The corresponding velocity vector fields are shown in Figure 3.

The direction of the velocity vectors is largely horizontal; the velocity is highest in the core of the spray and decreases radially outwards due to friction between the fast-moving spray and stationary surrounding air. The velocity also decreases as the distance from the spray orifice exit increases due to friction with atmospheric air. It is noted that the PIV representation of the flow field becomes very sparse at 150 ms and 200 ms. Figure 2 showed that the spray is much less dense as the propellant runs out. The spray also becomes intermittent and PIV image pairs cease to yield meaningful velocity information due to the low concentration of droplets.

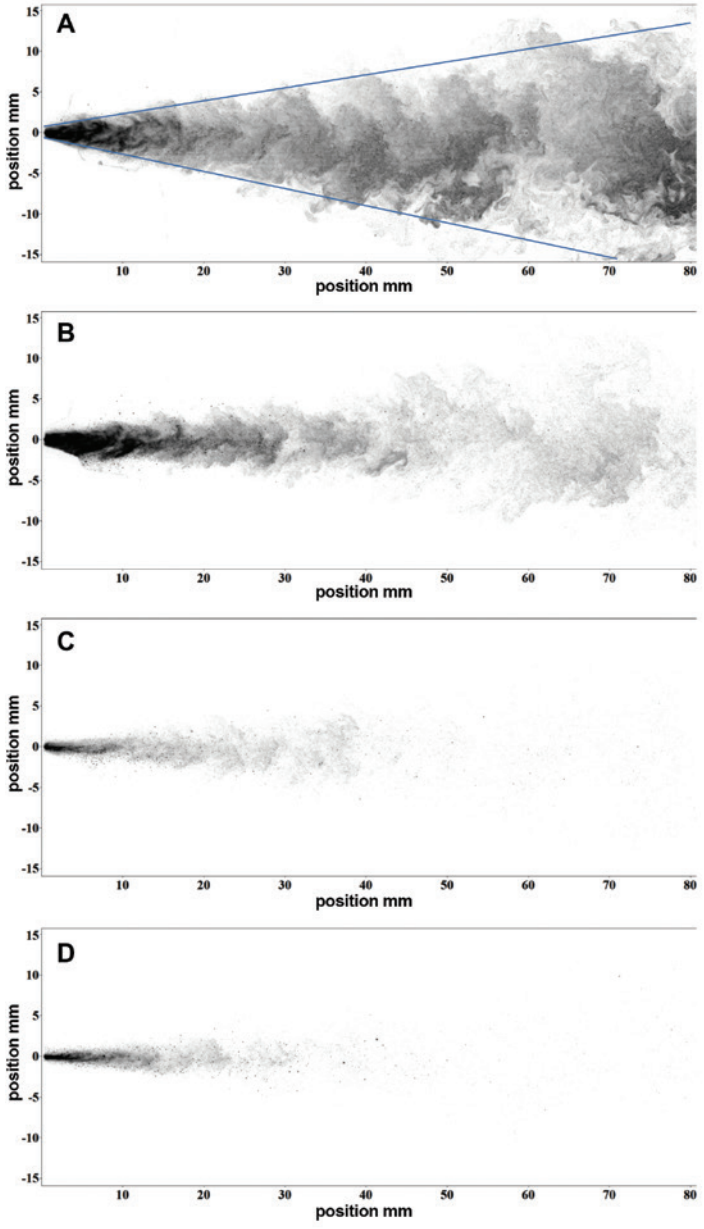

Figure 2. **Instantaneous far-field images of HFA134a spray. A) 50 ms (spray edge: 98% of pixel intensity counts inside boundaries), B) 100 ms, C) 150 ms, D) 200 ms.**

PDA – Spray Dynamics: Droplet Velocity

Figure 4 shows the temporal distribution of the axial velocity of a HFA134a aerosol plume measured by PDA (averaged over N = 10 spray events) and PIV (averaged over N = 5 spray events) at 25 mm from the spray orifice on the nominal spray centerline. The temporal profile shows a high initial velocity followed by a rapid drop to a minimum around 30-40 ms. The velocity gradually increases to a maximum around 100-120 ms and subsequently drops gradually towards zero over a period

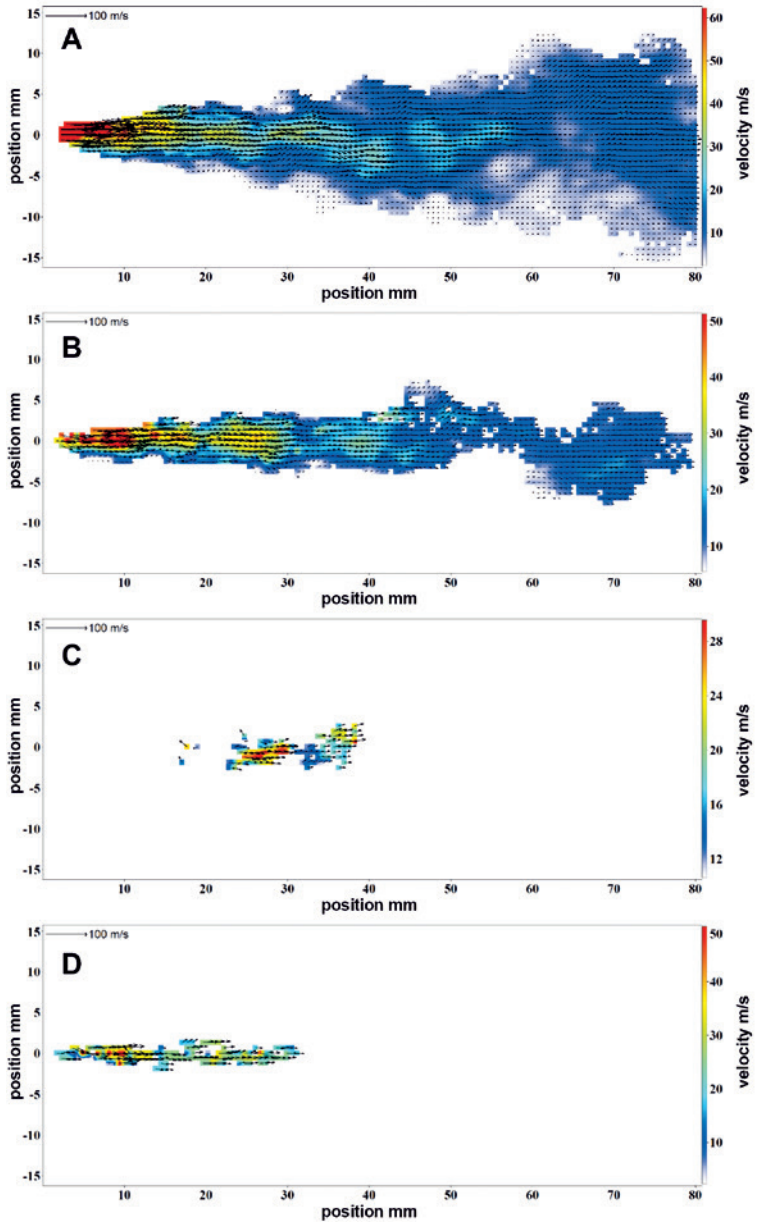

Figure 3. PIV velocity vector field of HFA134a spray (A) 50 ms, (B) 100 ms, (C) 150 ms, (D) 200 ms.

of several hundred milliseconds as the last remnants of formulation leave the actuator. This trend follows the changes of sonic velocities of the vapor-liquid flow through the spray orifice and was first predicted by Clark [9] and inferred from analysis of his spray thrust measurements. The trends agree favorably with those reported in [10-14].

Furthermore, it should be noted that the velocities measured by PDA and PIV are in close agreement throughout the spray event except after 200 ms, where PIV does not yield velocity information.

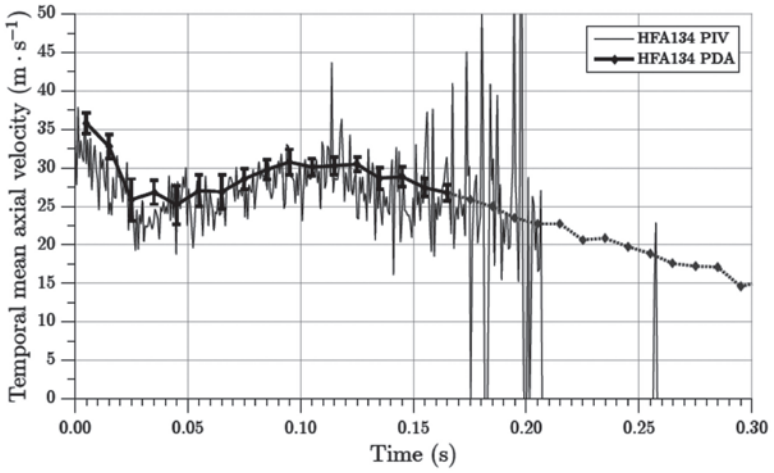

Figure 4. **Comparison of PDA and PIV temporal distribution of axial velocity of HFA134a spray on the nominal centerline at 25 mm from spray orifice.**

PDA and PIV data at varying radial distance y from the spray centerline at an axial distance of 25 mm from the spray orifice were processed to yield event-averaged velocity $u(y)$. The resulting values were non-dimensionalized by dividing each velocity $u(y)$ by the centerline velocity u_{max}. The non-dimensionalized velocity distribution for HFA134a and HFA227ea sprays is presented in Figure 5 as a function of non-dimensionalized radial location $y/y_{0.5}$, where $y_{0.5}$ is the so-called half width of the spray. This is the distance at which the velocity is equal to half the centerline velocity, i.e., $u(y_{0.5}) = 0.5u_{max}$. The non-dimensional presentation effectively highlights universal features of the flow field. Results presented in Figure 5 show that the non-dimensional velocity distribution was independent of formulation to within the experimental uncertainty.

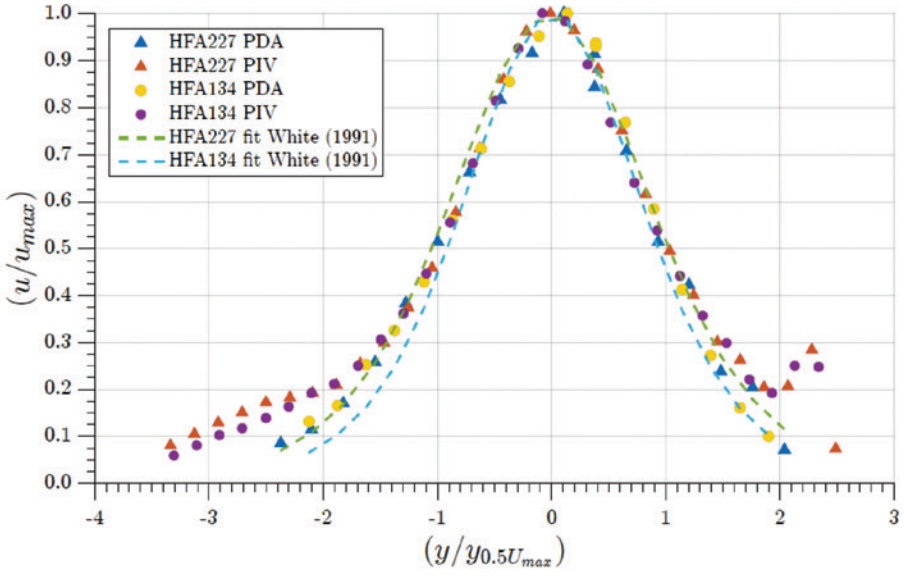

Figure 5. **Non-dimensionalized event-averaged velocity distribution as function of non-dimensionalized radius constructed from PDA and PIV results at 25 mm from spray orifice for HFA134a and HFA227ea sprays; dashed lines are based on theory for turbulent gas jets in White [15].**

In order to characterize the differences between the flow fields associated with various formulations, the event-averaged centerline velocity u_{max} as a function of the axial distance z from the spray orifice is presented in Figure 6. The event-averaged centerline velocity u_{max} is inversely proportional to the axial distance from a virtual source location, which is fairly close to the spray orifice exit. This relationship can be represented as follows: $u_{max}(z) = C/(z - z_0)$, where z = axial location, z_0 = virtual source location, C = spray velocity constant. Event-averaged centerline velocity data of sprays formed with all propellants and formulations studied in this work fell within ± 15% (dashed lines in Figure 6) around a non-linear best-fit line with this functional form using best-fit parameters C = 863 and z_0 = - 6.8 (solid line in Figure 6). The centerline velocities of HFA134a/ethanol mixtures were tightly bunched around the best-fit line, whereas those of the pure HFA227ea sprays were about 10% below the best-fit line as a consequence of the lower saturated vapor pressure of this propellant.

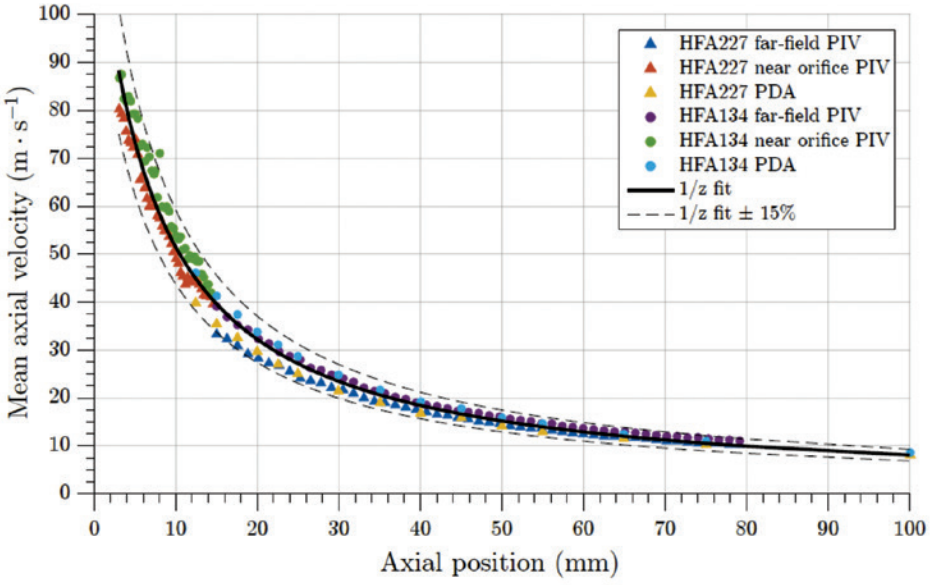

Figure 6. Event-averaged centerline velocity as function of distance from spray orifice exit based on PDA and PIV results for HFA134a and HFA227ea sprays.

The $1/(z\text{-}z_0)$ decay of the centerline and the self-similarity of the radial velocity distributions are familiar features of turbulent jets [16]. The present results suggest that turbulent mixing between the spray plume and the surrounding air also governs the spray dynamics at distances greater than 15-25 mm from the spray orifice.

Analysis of PIV Images – Cone Angle and Spray Direction

The cone angle and spray direction were obtained from analysis of the PIV images. The spray centerline is located where the velocity has a maximum u_{max}. The half-width $y_{0.5}$ is the distance from the centerline where the velocity is equal to half the centerline velocity, i.e. $u(y_{0.5}) = 0.5u_{max}$. The half width of the spray was found along a vertical line at an axial distance of 25 mm of each velocity vector field. The distances above and below the plume centerline to the points where $u = 0.5u_{max}$ represent the upper and lower plume half-widths $y_{0.5}$. The angle between lines projected from the top and bottom of the spray orifice to the plume half-width locations is the instantaneous cone angle. The angle between the bisector of these two lines and the spray centerline is the instantaneous spray direction.

The cone angle was found to vary between 12° and 24° and the spray direction ranged from -2° to +0.75°. Slow variations of the cone angle and spray direction occurred with a time scale around 50-100 ms. These were associated with filling and emptying of the actuator sump. Additional variations with short time scales around 5-10 ms were caused by variations of the spray orifice flow regime and exit conditions, as was also recently discovered by Honnery *et al.* [17] using X-ray techniques. The trends were similar to those found by Crosland *et al.* [13] from their PIV data. However, the cone angle in the present work was generally larger, but the variations of spray direction were smaller than those in [13]. Differences are likely to be due to geometric difference between the actuators; in particular, the spray orifice diameter was 0.5 mm in [13] and 0.3 mm in the present work.

It is interesting to note that the far-field cone angles were considerably larger than those of turbulent jets for a considerable fraction of the spray event, which indicates enhanced mixing in pMDI sprays. Moreover, the far-field cone angles were always considerably smaller than the near-orifice values at corresponding times obtained from high-resolution images. This suggests that the physics governing the spray in the immediate vicinity of the spray orifice is more complex than the far-field flow structure due to choking of the vapor-liquid flow in the spray orifice and flash evaporation of superheated propellant as the choked spray emerges from the actuator nozzle.

PDA – Spray Dynamics: Droplet Size

Figure 7 shows the temporal distribution of the droplet size D_{10} averaged over N = 10 spray events on the centerline at 25 mm from the spray orifice exit plane of a HFA134a aerosol plume measured by the PDA.

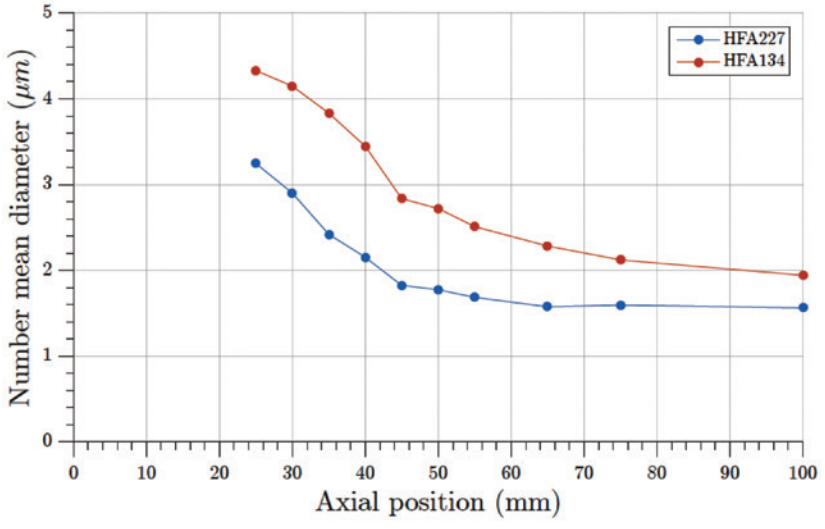

Figure 7. Event-averaged droplet size D_{10} on the centerline as a function of distance from the spray orifice exit for HFA134a and HFA227ea sprays.

The droplet diameter D_{10} shows a reduction with distance from the spray orifice as a result of propellant evaporation. The D_{10} for HFA227ea sprays was found to be 25-30% smaller than the corresponding value for HFA134a. This was against expectations, since the saturated vapor pressure of HFA134a is higher.

The corresponding distribution of event-averaged Sauter mean diameter (SMD) D_{32} showed erratic behavior. The SMD increased over the first 50 mm from the spray orifice. For HFA227ea sprays, the SMD reduces gradually over the next 50 mm. The maximum D_{32} for HFA134a occurs at a distance of 75 mm. The droplet size distribution was investigated further to investigate the cause of this behavior.

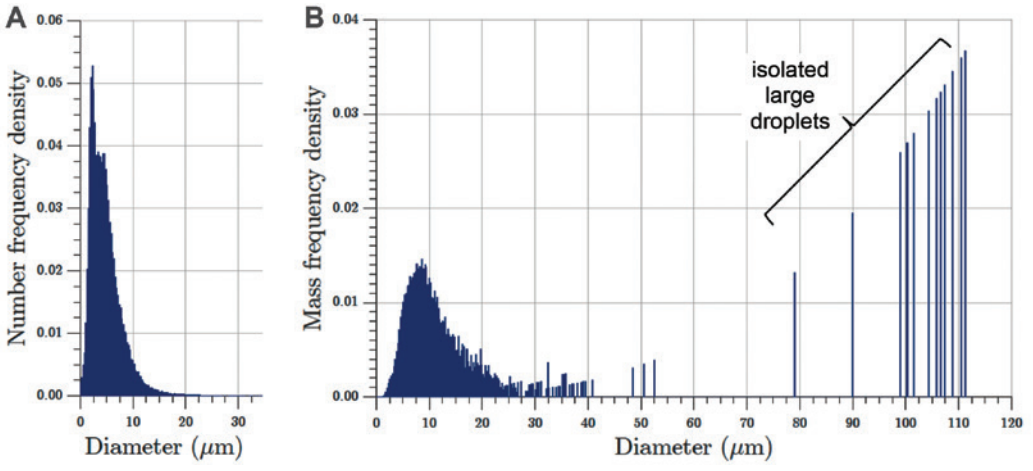

Figure 8. Distribution of event-averaged spray droplet size averaged over a plane at axial distance of 25 mm from the spray orifice exit for HFA134a. A) number frequency distribution, B) mass-weighted frequency distribution.

The mode of the number frequency distribution of droplet size is around 2.5 μm (Figure 8A), showing that the overwhelming number of droplets have respirable size at 25 mm from the spray orifice exit. Further analysis has shown that the distribution can be accurately represented by means of a log-normal distribution. Inspection of Figure 8A would suggest that the maximum droplet size is smaller than 20 μm.

The mode of the mass-weighted distribution of droplets with size below 50 μm is around 8 μm (Figure 8B). This falls within the range of initial MMD estimates in [3] (7-12 μm) for formulations with 1-20% w/w ethanol. The frequency distribution in Figure 8B also shows a large contribution due to individual droplets with diameter above 50 μm. The spray images discussed earlier revealed that the generation of large droplets took place at the edge of the spray, and, hence, is highly localized. The probability of detecting a representative sample of such droplets is low because there are so few of them and the PDA probe volume is very small. However, some very large droplets were indicated by the PDA measurements and, as shown, these individual droplets make a large contribution to the mass-weighted frequency distribution. This explains the erratic behavior of the reported SMD results.

Stein and Myrdal [3] did not find significant quantities of large droplets in measurements of the mass weighted particle size distributions of pMDI aerosols with the aerodynamic particle sizer. On the other hand, Smyth and Hickey [18] used laser diffraction and detected a bimodal size distribution with a peak of respirable particles with volume diameter around 1 μm and a second peak with non-respirable particles with size above 10 μm. It is interesting to note that these authors also reported a third peak with diameter around 100 μm, which was rejected as an artifact of beam steering due to high refractive index gradients in the spray plume. Further work is needed to confirm these results and research these contributions to the size distribution of the spray source in more detail. However, the present data may provide an alternative explanation for the third, rejected, peak in laser diffraction data.

CLOSING REMARKS

Particle deposition in the human airways is well correlated with the impaction parameter $\rho d_p^2 Q$ (ρ is the particle density, d_p is the mass median particle diameter and Q is the volumetric flow rate) [1, 19]. This implies that the product of particle size squared and velocity determines the amount and location of deposition. PDA makes simultaneous measurements of the size and velocity of a droplet, which is a unique advantage over other measurement techniques. The application of PDA to dense sprays, e.g., in the near-orifice region, can be problematic due to low validation rates and multiple scattering. Concerns have been raised about beam steering effects due to high refractive index gradients in pMDI sprays [17, 20]. The comparison of PDA and PIV results showed good agreement between velocities measured by the two techniques at distances greater than 15 mm from the spray orifice, which suggests that systematic errors are sufficiently well-controlled by the experimental protocol to have confidence in both measurements.

Properties of the event-averaged velocity distributions in the far-field were found to be in good agreement with those of turbulent gas jets [16] and fuel sprays [21] in the present work. This suggests that turbulent mixing plays a key role in the radial spreading of pMDI sprays. Large instantaneous variations of spray velocity, cone angle and spray direction found in this work are likely to increase the potential for oropharyngeal deposition in patients and also explains why significant deposition is found in the horizontal section of the USP induction port in cascade impactor measurements and can contribute to deposition in spacers and holding chambers.

Number mean and mode of the droplet size measured with PDA in the far-field region was found to be around 2-4 μm. The corresponding mass-weighted distribution showed a large contribution due to individual large droplets. Analysis of the spray images in the near field showed how these droplets are produced. Moreover, the cone angles were found to be much larger in the near-orifice region than in the far-field due to flash evaporation of superheated propellant in the near orifice region.

Sprays produced by pMDIs are highly dynamic with large changes of droplet size and spray velocity in the near-orifice and mouthpiece region. Study of the spray plume dynamics with optical diagnostics is challenging, but the application of phase-Doppler anemometry in conjunction with high-speed imaging and particle image velocimetry was highly effective and demonstrated the complementary nature of these instruments. Further research on pMDI sprays with these combined tools will provide insights into the processes responsible for changes in droplet size *and* velocity and contribute to understanding that can guide the development of the next generation of pMDI inhalers.

REFERENCES

1. Finlay WH: *The Mechanics of Inhaled Pharmaceutical Aerosols – An Introduction*, Academic Press, New York, NY: 2001.

2. Stein SW, Myrdal PB: The relative influence of atomization and evaporation on metered dose inhaler drug delivery efficiency. *Aerosol Sci Tech* 2006, 40(5): 335-47.

3. Stein SW, Myrdal PB: A theoretical and experimental analysis of formulation and device parameters affecting solution MDI size distributions. *J Pharm Sci* 2004, 93(8): 2158-75.

4. Fletcher GE: Factors affecting the atomisation of saturated liquids. PhD Thesis, Loughborough University of Technology, Loughborough, UK: 1975.

5. Buchmann NA, Duke DJ, Shakiba SA, Mitchell DM, Stewart PJ, Traini D, Young PM, Lewis DA, Soria J, Honnery D: A novel high-speed imaging technique to predict the macroscopic spray characteristics of solution based pressurised metered dose inhalers. *Pharm Res* 2014, 31: 2963-74.

6. Myatt B, Lewis D, Church T, Brambilla G, Hargrave G, Versteeg H, Long E, Gavtash B: PDA Analysis of HFA/ethanol pMDI aerosols: An improved test protocol and new findings. In *Proc ICLASS 2015*, Tainan, Taiwan: 2015: A1-1-070.

7. Wigley G, Hargrave GK, Heath J: A high power, high resolution LDA/PDA system applied to gasoline direct injection sprays. *Part Part Syst Charact* 1999, 16(1): 11-19.

8. Westerweel J, Scarano F: Universal outlier detection for PIV data. *Exp Fluids* 2005, 39: 1096-1100.

9. Clark AR: Metered atomisation for respiratory drug delivery. PhD Thesis, Loughborough University of Technology, Loughborough, UK: 1991.

10. Dunbar CA, Watkins AP, Miller JF: An experimental investigation of the spray issued from a pMDI using laser diagnostic techniques. *J Aerosol Med Pulm Drug Deliv* 1997, 10(4): 351-68.

11. Dunbar CA: Atomization mechanisms of the pressurized metered dose inhaler. *Part Sci Technol* 1997, 15(3-4): 253-71.

12. Wigley G, Versteeg HK, Hodson D: Near-orifice PDA measurements and atomisation mechanism of a pharmaceutical pressurised metered dose inhaler. In *Proc ILASS-Europe 2002,* Zaragoza, Spain, 165-70: 2002.

13. Crosland BM, Johnson MR, Matida EA: Characterization of the spray velocities from a pressurized metered-dose inhaler. *J Aerosol Med Pulm Drug Deliv* 2009, 22(2): 85-97.

14. Alatrash A, Matilda E: Characterization of medication velocity and size distribution from pressurized metered-dose inhalers by phase Doppler anemometry. *J Aerosol Med Pulm Drug Deliv* 2016, 29(6): 501-13.

15. White F: *Viscous Fluid Flow*. McGraw-Hill, New York, NY: 1991.

16. Abramovich GN: *The Theory of Turbulent Jets*. MIT Press, Cambridge, MA: 1963.

17. Honnery D, Mason-Smith N, Duke DJ, Kastengren AL, Chen Y, Young PM, Traini D, Lewis DA, Edgington-Mitchell D: New insights into pMDI operation using synchrotron X-ray techniques. In *RDD Asia 2016. Volume 1.* Edited by Dalby RN, Peart J, Young PM, Traini D. DHI Publishing; River Grove, IL: 2016: 209-20.

18. Smyth HDC, Hickey AJ: Multimodal particle size distributions emitted from HFA-134a solution pressurized metered-dose inhalers. *AAPS Pharm-SciTech* 2003, 4(3): E38.

19. Grgic B, Finlay WH, Heenan AF: Regional aerosol deposition and flow measurements in an idealized mouth and throat. *J Aerosol Sci* 2004, 35(1): 21-32.

20. Mason-Smith N, Duke DJ, Kastengren AL, Stewart PJ, Traini D, Young PM, Chen Y, Lewis DA, Soria J, Edgington-Mitchell D, Honnery D: Insights into spray development from metered-dose inhalers through quantitative X-ray radiography. *Pharm Res* 2016 33: 1249-58.

21. Desantes JM, Payri R, Garcia JM, Salvador FJ: A contribution to the understanding of isothermal diesel spray dynamics. *Fuel* 2007, 86: 1093-101.